chemosensors

MDPI

Article

QCM-Based HCl Gas Detection on Dimethylamine-Functionalized Crosslinked Copolymer Films

Jinchul Yang [1,2] and Jinyoung Park [1,2,*]

[1] School of Applied Chemical Engineering, Kyungpook National University, 80 Daehak-ro, Buk-gu, Daegu 41566, Korea; whdns861223@knu.ac.kr
[2] Department of Polymer Science & Engineering, Kyungpook National University, 80 Daehak-ro, Buk-gu, Daegu 41566, Korea
* Correspondence: jinpark@knu.ac.kr; Tel.: +82-53-950-5624

Abstract: In this work, sensing behaviors and mechanisms of two crosslinked copolymers with dimethylamine and dimethylamide functional groups were compared and investigated for their ability to detect hydrogen chloride (HCl) gas. The crosslinked copolymer films were photopolymerized on quartz crystal electrodes using a micro-contact printing technique. The gas sensing behaviors were analyzed by measuring resonant frequency (Δf) of quartz crystal microbalance (QCM). The HCl binding capacity of photopolymerized films, with a mass between 4.6 and 5.9 μg, was optimized. Under optimized film mass conditions, the poly(2-dimethylaminoethyl methacrylate-co-ethylene glycol dimethacrylate) (DMAEMA-co-EGDMA), poly(DMAEMA-co-EGDMA), film, C2-DMA, showed a 13.9-fold higher binding capacity than the poly(*N*,*N*-dimethylacrylamide-co-ethylene glycol dimethacrylate, poly(DMAA-co-EGDMA), film, C0-DMA, during HCl gas adsorption. HCl gas was effectively adsorbed on the C2-DMA film because of the formation of tertiary amine salts through protonation and strong ionic bonding. Furthermore, the C2-DMA film exhibited excellent sensitivity, of 2.51 (ng/μg) (1/ppm), and selectivity coefficient (k^* = 12.6 for formaldehyde and 13.5 for hydrogen fluoride) compared to the C0-DMA film. According to the experimental results, and due to its high functionality and stability, the C2-DMA film-coated QC electrode could be used as an HCl gas sensor, with low-cost and simple preparation, in future endeavors.

Keywords: toxic gas; 2-dimethylaminoethyl methacrylate; quartz crystal microbalance

Citation: Yang, J.; Park, J. QCM-Based HCl Gas Detection on Dimethylamine-Functionalized Crosslinked Copolymer Films. *Chemosensors* **2022**, *10*, 70. https://doi.org/10.3390/chemosensors10020070

Academic Editors: Andrea Ponzoni and Salih Okur

Received: 29 December 2021
Accepted: 8 February 2022
Published: 10 February 2022

1. Introduction

Hydrogen chloride (HCl) gas is generated by incinerating chloride-containing materials, such as plastics (e.g., polyvinyl chloride), papers, and coals [1,2]. It has been recognized as one of the acid gas air pollutants due to its toxic effect on the environment and human health. Exposure to HCl gas can have adverse effects on the human body, including the eyes, mucous membranes, and skin. In addition, exposure to highly concentrated HCl gas (>100 ppm) can lead to acute laryngeal cramps or pulmonary edema [3]. Therefore, various types of gas sensors, including optochemical [4–8], colorimetric [9,10], amperometric [11], conductometric [12], and electrochemical [13] sensors, have been proposed to control and monitor HCl gas discharged into the atmosphere. In particular, quartz crystal microbalance (QCM) has been used as a sensing instrument to detect HCl gas because of the ease of quantitative analysis observed by converting a measured frequency variation into a mass change. In a QCM-based sensing system, various functional materials can be used on the QCM electrode in order to amplify the signal resulting from the binding reaction of analytes. In this context, Matsuguchi et al. reported three kinds of poly(acrylamide) derivative-coated quartz resonators for accurately detecting HCl gas in the air [14]. They found that the sensitivity, response time, and reversibility of resonators depend on the chemical structure of the amide group, and they concluded that poly(*N*,*N*-dimethylacrylamide) (PDMAA)

among the used polymers was the best suited for HCl sensors when considering the relevant data measured using a QCM instrument. Furthermore, they have used various functional polymer-based materials, such as electrodeposited polymer [15], fluorescent polymer [16], poly(*N*-isopropylacrylamide) (PNIPAM) nanoparticles (NPs) [17–19], and PNIPAM brushes [20,21] to detect HCl gas. Despite extensive efforts to develop polymer-based gas sensors, a fabrication process which includes greater simplicity and lower cost should be required to produce efficient gas-sensing platforms. In this regard, our group has previously reported aminated polystyrene (a-PS) colloids, which could be prepared through a simple substitution process to detect HCl gas [22]. Secondary amine salts were formed on the QCM sensors with the a-PS colloids through the reaction between a secondary amine group and HCl gas, resulting in a high binding capacity, of 102 μg/mg, and excellent sensitivity and selectivity. Here, we concluded that the structure of the amine group can influence HCl adsorption properties. However, it was difficult to immobilize spin-coated colloids on quartz crystal (QC) electrodes for the development of QCM-based HCl gas sensors. Moreover, the harsh treatment, with a toxic acid, was essentially required to attach amine groups on the PS colloids.

As an extension of our previous study, we used 2-dimethylaminoethyl methacrylate (DMAEMA) to develop a QCM-based HCl gas-sensing crosslinked copolymer film. The tertiary amine salt is formed by a chemical reaction between the tertiary amine groups of DMAEMA and HCl. As a crosslinking monomer, ethylene glycol dimethacrylate (EGDMA) was used for sufficient polymer film stability; thus, poly(DMAEMA-co-EGDMA) films, denoted by C2-DMA, were prepared on quartz crystal (QC) substrates through ultraviolet (UV) radical polymerization. The mass dependence of the copolymer film was confirmed by comparing HCl-binding capacities on the films fabricated in various masses. Using *N*,*N*-dimethylacrylamide (DMAA), proven to be a suitable functional monomer of HCl sensors, poly(DMAA-co-EGDMA) films, i.e., C0-DMA, were also produced as control samples. This copolymer film can interact with HCl gas on the carbonyl group of the tertiary-amide group. Therefore, the HCl adsorption behavior of the two copolymer film types, containing different functional groups (i.e., tertiary amine and amide), was comparatively analyzed. Furthermore, adsorption characteristics, e.g., the binding capacity, oxygen/moisture dependence, sensitivity, and selectivity of the two film types, were investigated using a QCM instrument under flowing HCl gas.

2. Materials and Methods

2.1. Materials

Both functional monomers, DMAEMA and DMAA were purchased from Tokyo Chemical Industry Co., Tokyo, Japan. Ethylene glycol dimethacrylate (EGDMA) and 1-hydroxycyclohexyl phenyl ketone (HCPK), purchased from Tokyo Chemical Industry Co., Japan, were used as the crosslinking monomer and the photoinitiator, respectively. Dry gas mixtures (≈100 μmol/mol $HCHO/N_2$, HF/N_2, and HCl/N_2) and synthetic air were obtained from Korea Standard Gas Co., Daegu, Korea. All materials were used as received, without further purification.

2.2. Fabrication of Poly(2-dimethylaminoethyl methacrylate-co-ethylene glycol dimethacrylate) Film

Poly(DMAEMA-co-EGDMA) films were fabricated through UV radical polymerization (Figure 1a). First, DAMEMA (950 mg), EGDMA (40 mg), and HCPK (10 mg, initiator) were orderly injected into a 5-mL vial. After ultrasonication for 5 min, a 0.1-μL well-mixed solution was dropped onto a 9-MHz gold-coated AT-cut QC (QA-A9M AU, M, Seiko Instruments Inc., Tokyo, Japan) substrates using a micropipette. Then, a polyethylene terephthalate (PET) film was covered on the QC substrates, under a certain pressure, to form a smooth planar film over the entire area, and, sequentially, photopolymerization was performed using a UV lamp (365 nm, 36 W) for 5 min. After physical detachment of the covered PET film, the QC substrates were dried at room temperature for 1-h. The

mass of crosslinked films coated on the QC electrodes was adjusted by controlling induced pressure during micro-contact printing, and it was calculated from a change in resonant frequency (Δf) of QC electrode. Several crosslinked polymer films, in the mass range of 1.7–11.8 μg (film thickness = 104–547 nm), were prepared in order to find film coating conditions with optimized thickness for obtaining the maximum sensing signal (Figure S1). As comparable samples, C0-DMA films were prepared through the same procedures using DMAA monomers.

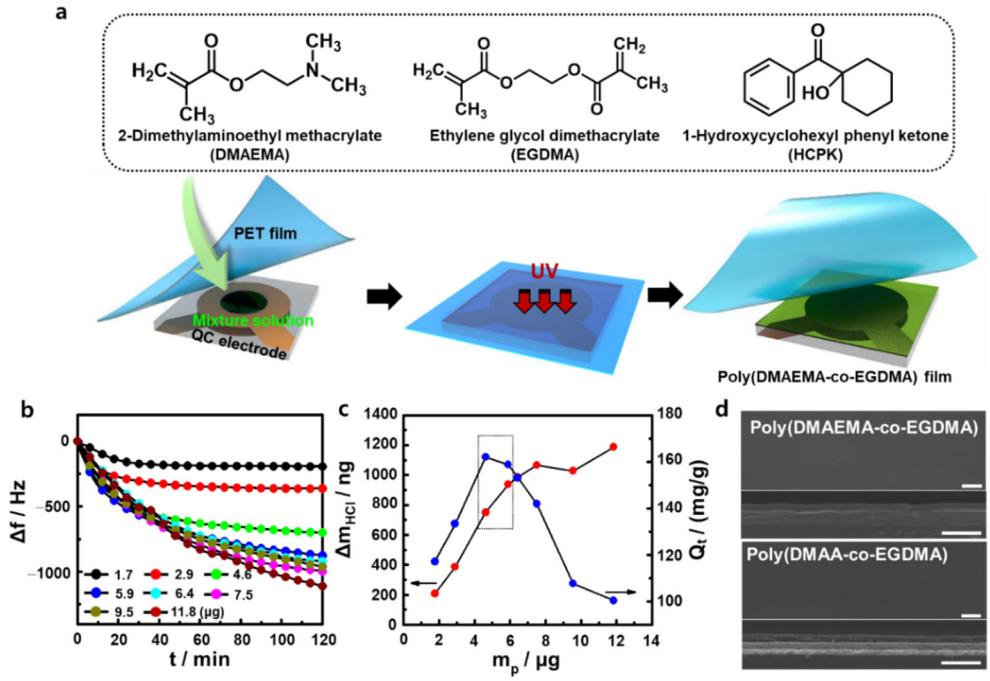

Figure 1. (**a**) Fabrication process of poly(2-dimethylaminoethyl methacrylate-co-ethylene glycol dimethacrylate), poly(DMAEMA-co-EGDMA), film via photopolymerization. (**b**) Resonant frequency change (Δf) as a function of adsorption time of poly(DMAEMA-co-EGDMA) films, ranging from 1.7 to 11.8 μg, in 70-ppm HCl gas flow, at 22 °C and 10% RH. (**c**) Mass change (Δm) and binding capacity (Qt) as a function of film mass of poly(DMAEMA-co-EGDMA) film in 70-ppm HCl gas flow, at 22 °C and 10% RH. (**d**) SEM images for poly(DMAEMA-co-EGDMA) and poly(*N*,*N*-dimethylacrylamide-co-EGDMA), poly(DMAA-co-EGDMA), films (above: top view; bottom: cross-sectional view). All scale bars are 1 μm.

2.3. Adsorption Properties

The surface morphology and dimensions of copolymer films were characterized using field emission scanning electron microscopy (FE-SEM, Hitachi SU 8220, Tokyo, Japan). A Fourier transform infrared (FT-IR) spectrometer (FT-IR-4100, Jasco Inc., Easton, MD, USA), with an attenuated total reflectance (ATR, PRO450-S) accessory, and an X-ray photoelectron spectrometer (XPS, NEXSA, Thermo Fisher, Waltham, MA, USA), with an Al-Kα X-ray source (1486.6 eV), were used to investigate adsorption behaviors after HCl adsorption, which were related to the chemical structure and functional groups of copolymer films. The Δf value of two copolymer films was monitored using a QC analyzer (QCA 922, Seiko EG&G, Seiko instruments Inc., Tokyo, Japan), under flowing HCl gas, controlled using a remote-control software installed on a mass flow controller (MFC, i-300CV-V4). The adsorption experiments were conducted, in the concentration range of 10–70 ppm, at atmospheric pressure with an ambient temperature of 22 °C and relative humidity (RH) of 10%. Each gas concentration was modulated by mixing synthetic air, of 21–450 standard cubic centimeters per minute (sccm), and main toxic gases, of 50 sccm. For the selectivity test, the Δf values were measured, flowing 70-ppm each dried gas, i.e., HCl, formaldehyde (HCHO) and hydrogen fluoride (HF), in the same gas flowing system.

The Δf value was converted into the mass deposited on the surface of the copolymer films using the Sauerbrey equation [23] as follows:

$$\Delta f = \frac{-2f_0^2 \Delta m}{A\left(\rho_q \mu_q\right)^{1/2}} \quad (1)$$

where Δf and Δm represent the resonant frequency change (Hz) and mass change (ng), respectively. The f_0 represents the fundamental resonant frequency of QCM, ρ_q represents the density of quartz, μ_q represents the shear modulus of the crystal's material, and A represents the active area of the crystal. The sensitivity factor of the 9-MHz AT-cut gold-coated QC substrate was approximately 0.1834 Hz cm^2 ng^{-1}. Considering the defined active area (A = 0.19625 cm^2), the mass change is calculated as 1.07 ng, corresponding to a frequency shift of 1 Hz.

3. Results

The mass of the copolymer film coated on the QCM electrode is an important factor affecting the adsorption capacity and diffusion coefficient in the HCl adsorption process. An ultrathin copolymer film can cause an insufficient signal for HCl adsorption, whereas, in the case of extremely thick film, the diffusion rate may be very slow, even if the detection signal is amplified. Thus, the mass dependence of the C2-DMA film coated on the QCM electrode should be optimized to maximize the adsorption signal. In this regard, various copolymer films, with a mass range of 1.77–11.83 μg, were investigated, monitoring Δf values under a 70-ppm HCl gas flow. As shown in Figure 1b, the Δf values of copolymer films with a mass up to 7.5 μg were linearly increased as a function of adsorption time, and this occured because of an increase in adsorption sites for the HCl gas. However, the Δf value of the C2-DMA film with a mass of 9.5 μg was slightly reduced because of the relatively lower diffusion rate at the thick film. Figure 1c depicts HCl mass and adsorption capacity (Q_t) value, in 2-h adsorption, pertaining to various C2-DMA masses on the films. The film with a mass of 4.6 μg had the highest Q_t value (162 mg/g). As a comparison sample, a C0-DMA film was also prepared with a mass range of 5.1–5.5 μg. The thicknesses of the C2-DMA (m_p = 5.54 μg) and C0-DMA (m_p = 5.11 μg) films were 227 ± 8.9 and 195 ± 16.6 nm, respectively (Figure 1d).

To investigate the adsorption response for each crosslinked film, Δf values were recorded while flowing dry HCl of 70 ppm in a chamber until the frequency reached an equilibrium state in the process of adsorption (2-h for C2-DMA and 10-min for C0-DMA) and desorption (10-min for both films). Figure 2 and Figure S2 show Q_t and Δf values as a function of time for two different films. In both crosslinked films, the Q_t values gradually increased with time, owing to HCl adsorption toward functional groups on each film. The C2-DMA film exhibited an equilibrium adsorption capacity (Q_e) value of 161.7 ± 2.8 ng/μg in the equilibrium state, and a 13.9-times-higher adsorption signal than C0-DMA film (11.6 ± 0.3 ng/μg). The significantly increased adsorption response depended highly on the functional group of the copolymer film. The tertiary amine groups of the DMAEMA could interact with HCl molecules through strong chemical bonds, forming tertiary amine salts, whereas the carbonyl groups of the DMAA may form relatively weak hydrogen bonds with HCl gas. The origin of different interactions resulted in vastly different desorption behaviors.

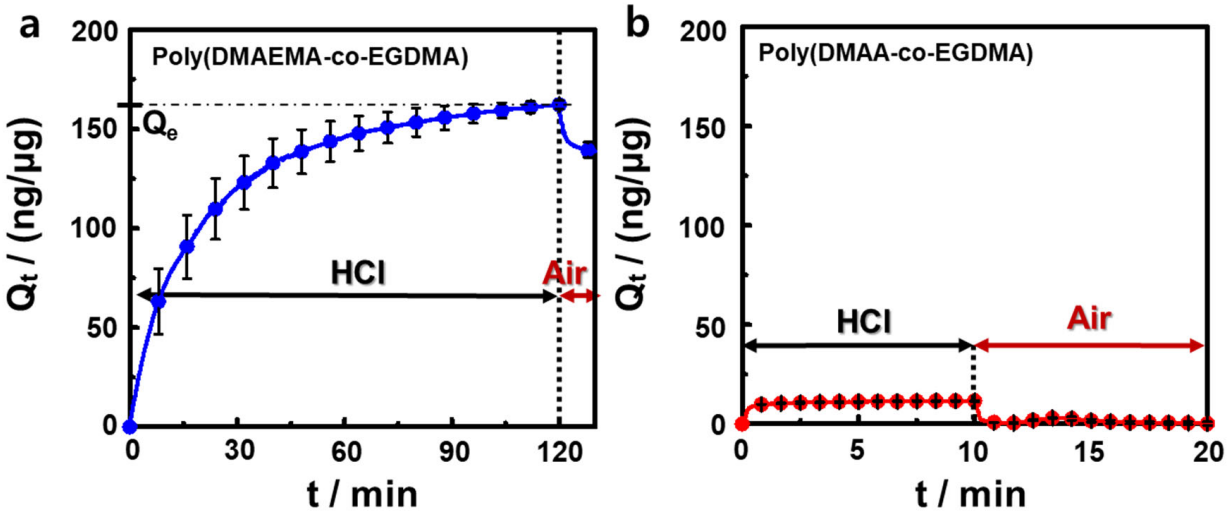

Figure 2. Binding capacity (Q_t) as a function of time for (**a**) poly(DMAEMA-co-EGDMA) and (**b**) poly(DMAA-co-EGDMA) films in 70-ppm HCl, and synthetic air flow at 22 °C and 10% RH during the adsorption process. Synthetic air was used for desorption. The adsorption–desorption process was performed until the signal stabilized.

In order to confirm the desorption behavior of the two copolymer films, the recovery value (R_e) was calculated using the following equation:

$$Re\ (\%) = \frac{Q_e(\mathrm{HCl}) - Q_e(\mathrm{air})}{Q_e(\mathrm{HCl})} \times 100 \quad (2)$$

where Q_e(HCl) is the equilibrium binding capacity after the binding process of HCl gas and Q_e(air) is the equilibrium binding capacity after flowing synthetic air. The adsorption signal of the C0-DMA film was almost restored to its original state, with a *Re* value of 98.8%, during the air flowing process due to the easy desorption of HCl gas caused by a weak hydrogen-bonding interaction between carbonyl groups and HCl molecules (Figure 2b). However, the *Re* value of the C2-DMA film was extremely low, approximately 14.3%, because of an irreversible reaction between the tertiary amine groups of the copolymer film and HCl gas; in other words, this irreversible adsorption–desorption behavior was derived from strong ionic bonding between protonated tertiary amine groups of DMAEMA and chloride ions (Figure 2a). The film might be recovered through post-treatment by immersing it in NaOH aqueous solution to eliminate the bound Cl^- ions [22]. However, the C2-DMA film could be used only as disposable HCl gas; this is because of low film stability on the electrode in the recovery process. Similar adsorption–desorption behaviors were exhibited on both the films while flowing 100 ppm HCl gas for three-cycles (Figure S3). The Δf value of C0-DMA was almost recovered as initial value according to the elapsed cycle. However, the Δf value of C2-DMA was accumulated by binding HCl gas without restoration during the desorption process. The *Re* values for C2-DMA and C0-DMA were 95.3% and 12.4%, respectively.

In order to gain further understanding of the interaction mechanisms between polymer films and gas analytes, XPS wide-scan spectra were performed, with two different films, before and after HCl adsorption (Figure S4). Three sharp peaks were observed in the C0-DMA film at 532.08 eV for O 1s, 400.08 eV for N 1s, and 285.08 eV for C 1s before the HCl adsorption process. After HCl adsorption, no signals appeared, and this was related to HCl adsorption, because of the detachment of unstable adsorbed HCl molecules in ambient conditions. However, a new peak corresponding to the Cl 2p signal was observed at 198.08 eV in the C2-DMA film after the adsorption process, confirming that the HCl analyte irreversibly interacted with DMAEMA. More specifically, Figure 3a illustrates the high-resolution XPS N 1s spectra ranging between 394 and 406 eV for the two films. In the

C0-DMA film, only one peak corresponding to the tertiary-amide nitrogen was observed at 399.78 eV for preadsorption and 399.48 eV for postadsorption. In contrast, the C2-DMA film exhibited one peak at 398.78 eV due to neutral nitrogen atoms in tertiary amine groups, whereas a new peak appeared at 401.58 eV, implying positively charged amine (N^+) in tertiary ammonium salt after the HCl adsorption process [24]. Furthermore, the XPS Cl 2p scan spectra of the two films are presented in Figure 3b. No noticeable peaks were observed on both the films at HCl preadsorption. However, after HCl adsorption occured on the C2-DMA film, two clear peaks including $2p_{3/2}$ and $2p_{1/2}$ chloride ion (Cl^-) were observed at 197.08 and 198.38, respectively [25]. These results were reconfirmed, via FT-IR spectra, before and after HCl adsorption. As shown in Figure 3c, a strong peak was observed at 1618 cm^{-1}, and this was associated with CO–N stretching on the IR spectrum of the C0-DMA film before HCl adsorption. The absorption bands at 1496, 1354, and 1138 cm^{-1} are attributed to the C–H bending, C–N stretching, and C–O stretching, respectively. The two weak peaks can be assigned to the O–H stretching and C–H stretching at 3464 and 2927 cm^{-1}, respectively. Interestingly, two IR spectra of the C0-DMA film before and after HCl adsorption were almost overlapped, on the basis of the CO–N stretching peak at 1628 cm^{-1}, because there was no chemical interaction between HCl gas and the amide-based film. In the case of C2-DMA film, the absorption peaks were observed at 1723, 1455, and 1146 cm^{-1} for C–O stretching, C–H bending, and C–O stretching vibration, respectively. The peaks in ranges of 2944–2769 cm^{-1} were ascribed to the C–H stretching of tertiary amine. Remarkably, for the C2-DMA film, N–H and C–H stretching peaks appeared in ranges of 3410 to 2463 cm^{-1}, owing to protonation on tertiary amine groups, which is similar to the FT-IR peaks of pure triethylamine hydrochloride [26].

As shown in Figure 4a,b, HCl adsorption (2-h for C2-DMA and 10-min for C0-DMA) and desorption (10-min for both films) behaviors of crosslinked films were investigated while flowing three individual carrier gases, i.e., dried N_2 (RH 10%) or synthetic air (RH 10% or 50%), including 50-ppm dried HCl, to identify the effects of oxygen and moisture on the adsorption response. For the C2-DMA film, the Q_e values for 2-h HCl adsorption were 150.7 $\pm$ 7.1 ng/μg in N_2 and 148.0 $\pm$ 9.1 ng/μg in the air, respectively. Considering that the protonated tertiary ammonium salt ionically bonded with the HCl analyte during the adsorption process, the adsorption response did not exhibit any significant difference, and this finding occurred, notably, in the presence of oxygen in the HCl/air–gas mixture. After the desorption process through air gas flow, the Q_e value was not recovered, and this was because of the strong bonding of the HCl analyte to the film. At high RH (50%), the Q_e value was approximately 100-ng/μg higher than that at the other conditions (RH 10%), owing to the effect of a signal increase which was caused by water moisture adsorbed on the film [27]. However, the Q_e value decreased to 168.8 $\pm$ 1.4 ng/μg after 10-min desorption process, nearly reaching the value reflected by adsorbed HCl mass itself, with no moisture effect, because the adsorbed moisture on the film was removed. In contrast, the Q_e value of the C0-DMA film in the dried air (7.26 $\pm$ 0.7 ng/μg) showed a 0.45-fold decrease compared with that in the N_2 gas (15.9 $\pm$ 3.5 ng/μg), and this was due to the interference effect of oxygen on the hydrogen bond between the carbonyl group and HCl. In addition, the increase in Q_e value caused by the adsorption of water molecules also occurred on the C0-DMA film at high RH (50%). After the desorption process, Q_e values became zero, indicating that few HCl molecules, weakly bonded on the film, were easily removed; thus, this film exhibited a worse adsorption response than the C2-DMA film.

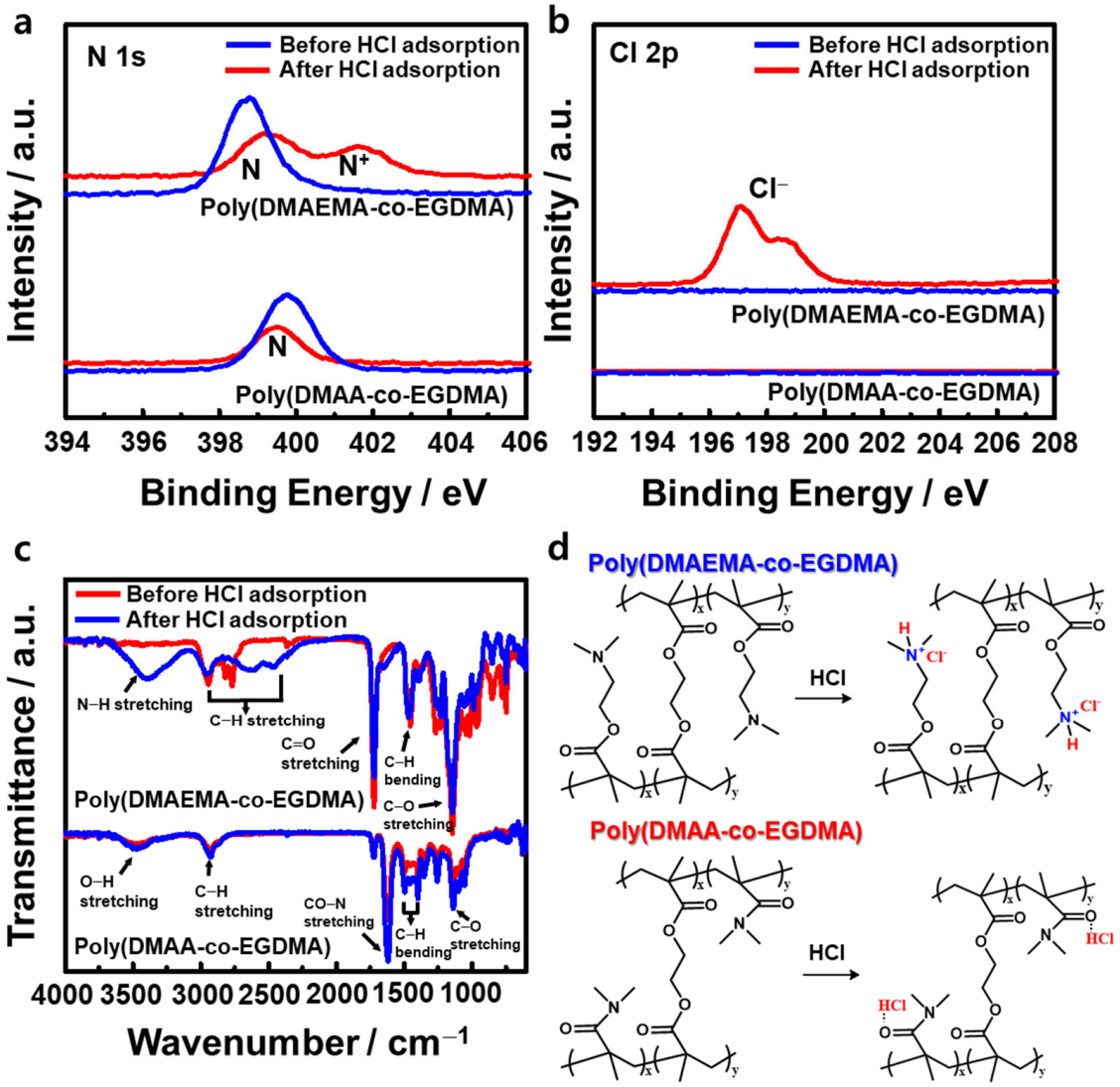

Figure 3. (**a**,**b**) High-resolution X-ray photoelectron spectra for (**a**) N 1s and (**b**) Cl 2p on poly (DMAEMA-co-EGDMA) and poly(DMAA-co-EGDMA) films before and after HCl adsorption and (**c**) Fourier transform infrared spectra for poly(DMAEMA-co-EGDMA) and poly(DMAA-co-EGDMA) films before and after HCl adsorption. (**d**) Predicted HCl adsorption mechanism on poly(DMAEMA-co-EGDMA) and poly(DMAA-co-EGDMA) films.

As shown in Figures 4c,d and S5, the 2-h adsorption responses, i.e., Q_e and Δf values, were studied with respect to an HCl gas concentration ranging from 10 to 70 ppm in order to determine the concentration dependence of the two crosslinked films. As shown in Figures 4c and S5a, the Q_e and Δf values of the C2-DMA film were significantly increased within the HCl concentration range of 10–50 ppm, and they were saturated at higher concentrations (>50 ppm). On the other hand, for the C0-DMA film, the adsorption responses gradually increased with an increase in the concentration of HCl gas (Figures 4d and S5b). A linear regression curve of the C2-DMA film, for adsorption at a concentration range of less than 50 ppm, is shown in the inset of Figure 4c. Its sensitivity was calculated to be 2.51 (ng/μg)(1/ppm) with a coefficient of determination (R^2) of 0.977, indicating that it was 14.8-fold higher than the C0-DMA film with 0.17 (ng/μg)(1/ppm) and R^2 = 0.984. The sensitivity of the C2-DMA film could also be obtained from the linear regression curve in the plot of Δf value as a function of HCl concentration in ranges of 10–50 ppm (Figure S6). The sensitivity (13 Hz/ppm) of the C2-DMA film was much higher than other sensors in previously reported studies (Table S1). Furthermore, the limit of quantitation (LOQ), and

the limit of detection (LOD), for the two copolymer films were determined using equations such as LOQ = 10 S/m and LOD = 3.3 S/m, where S represents the standard deviation of the y-intercept, and m represents the slope of the linear calibration curve [28,29]. LOQ and LOD values of 1.67 and 0.55 ppm were obtained for the C2-DMA film, and 4.84 and 1.59 ppm for the C0-DMA film, respectively.

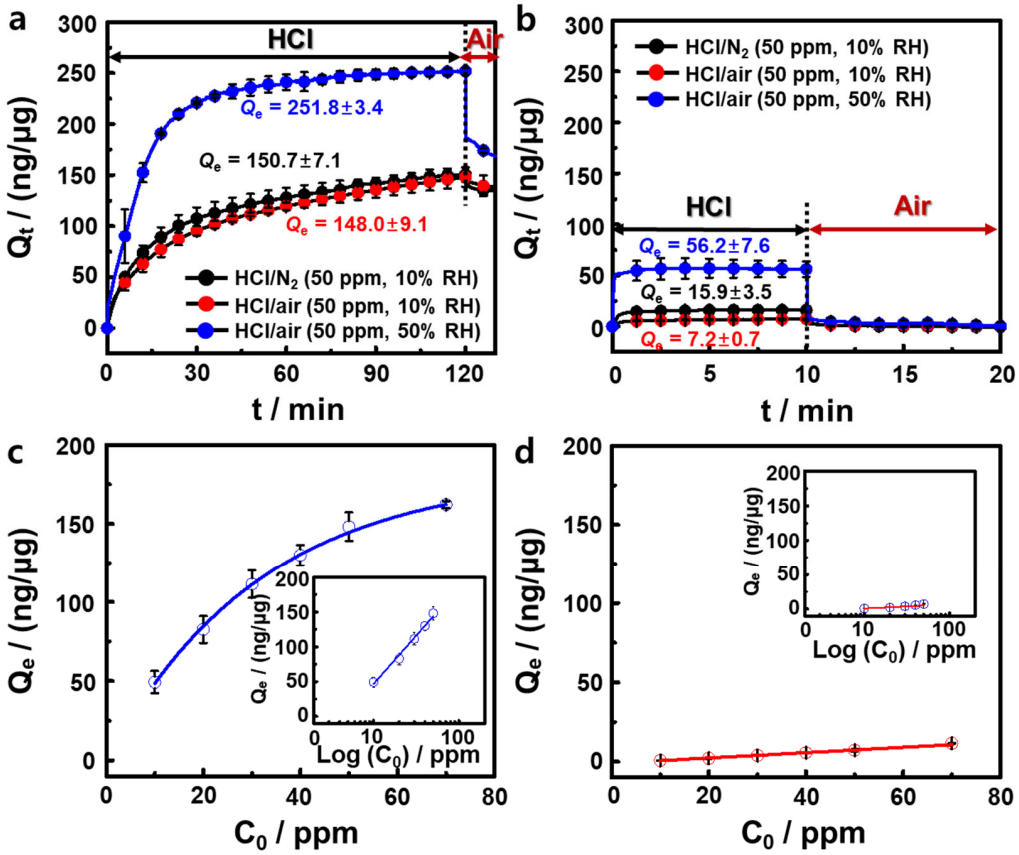

Figure 4. (**a**,**b**) Binding capacity (Q_t) as a function of time for (**a**) poly(DMAEMA-co-EGDMA) and (**b**) poly(DMAA-co-EGDMA) films in 50-ppm HCl with various carrier gases, i.e., dried N_2 (10% RH) and synthetic air (10% and 50% RH) at 22 °C during the adsorption process. Synthetic air was used for desorption. The adsorption–desorption process was performed until the signal stabilized. (**c**) Equilibrium binding capacity (Q_e) for (**c**) poly(DMAEMA-co-EGDMA) and (**d**) poly(DMAA-co-EGDMA) films as a function of initial concentration (C_0) of HCl gas ranging from 10 to 70 ppm at 22 °C and 10% RH after the adsorption process. The inset of Figure 4 represents the Q_e for two films as a logarithmic function of the initial concentration of HCl gas flow ranging from 10 to 50 ppm.

Furthermore, the Langmuir and Freundlich isotherm models were used to compare the adsorption behavior of the two films. The Langmuir isotherm model assumes that adsorption behavior is based on monolayer adsorption on a solid surface, which has a homogeneous surface for the target molecules. However, the Freundlich isotherm describes multilayer adsorption for a heterogeneous surface. Equations (3) and (4) describe the Langmuir and Freundlich models, respectively [30,31]:

$$Q_e = \frac{k_L C_e Q_m}{1 + k_L C_e} \tag{3}$$

$$Q_e = k_F C_e^{1/n} \tag{4}$$

where Q_e (mg/g) is the equilibrium adsorption capacity, C_e (mg/L) is the equilibrium concentration of HCl during adsorption, Q_m (mg/g) is the maximum adsorption capacity,

$1/n$ is a factor used to evaluate surface heterogeneity, and k_L and k_F represent the Langmuir and Freundlich adsorption equilibrium constants, respectively.

Figure 5 depicts the nonlinear fitted curves of the Langmuir isotherm and Freundlich isotherm models, respectively, pertaining to HCl adsorbed on the surface of the two films during the adsorption process. The parameters of the two isotherm models are presented in Table S2. Based on R^2 values, the experimental data points of the C2-DMA film were better fitted to the Langmuir model than the Freundlich isotherm model. This result indicates that only one HCl molecule is adsorbed at a tertiary amine group of the copolymer film. For the C0-DMA film, the experimental data points were not fitted to both models due to low Q_e values caused by the small adsorption response for HCl adsorption. According to these results, the experimental data of the C2-DMA film were well fitted to the Langmuir linear model because the copolymer film is based on a stoichiometric chemical reaction with HCl gas.

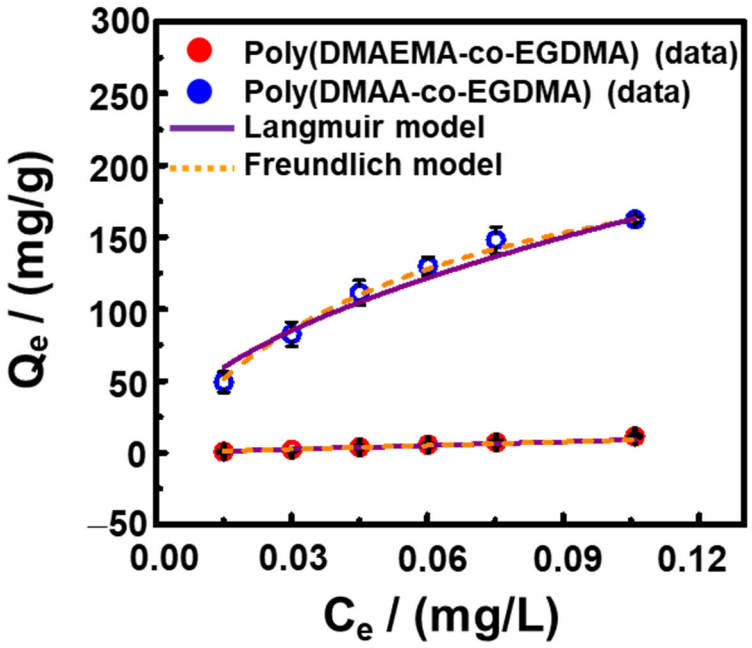

Figure 5. Nonlinear and linear adsorption isotherm curves for poly(DMAEMA-co-EGDMA) and (DMAA-co-EGDMA) films. Experimental data were obtained from the conversion of the resonant frequency change (Δf) in 10–70-ppm HCl gas flow, at 22 °C and 10% RH.

In order to evaluate the selective adsorption performance of the two crosslinked films, Δf values by gas adsorption and/or desorption were monitored, flowing 70 ppm each gas of HCHO and HF, including HCl in a chamber until the sensing signal was stabilized in the process of adsorption (2-h for C2-DMA and 10-min for C0-DMA) and desorption (10-min for both films) (Figure 6). On the C2-DMA film, the Δf value with HCl gas adsorption reached approximately −767 Hz, whereas the value was maintained at -61.6 ± 6.6 Hz for HCHO gas adsorption and -57.4 ± 11.4 Hz for HF gas adsorption in a 2-h gas flow. With regard to the desorption process under air gas flow, the Δf value was slightly decreased before it stabilized because of the irreversible binding of HCl molecules. However, the Δf value was approximately zero in nonselective adsorption of other gases (Figure 6a). Furthermore, on the C2-DMA film, Q_e values were 12.9 ± 1.4 and 12.0 ± 2.4 ng/μg for the HCHO and HF gases, respectively, which are extremely low compared with the adsorption response of HCl gas (162.1 ± 2.2 ng/μg) (Figure 6a). The selectivity coefficient (k^*), as the ratio of the $Q_{e,HCl}/Q_{e,(HCHO\ or\ HF)}$, was especially high, with numbers of 12.6 and 13.5 for the HCHO and HF gases, respectively, because HCl gas reacts by protonation and ionic bonding toward the tertiary amine groups. In addition, the R_e values for HCHO and HF were 103.5% and 99.9% after the desorption process of the adsorbed toxic gas, and this

was due to the breakdown of hydrogen-bonding interactions. In contrast, the adsorption response on the C0-DMA film for 10-min was extremely low, with a Δf value between −39 and −61 Hz, regardless of the type of toxic gas. Q_e values were 11.6 ± 0.3, 9.8 ± 0.4, and 8.0 ± 0.3 ng/μg for the HCl, HCHO, and HF gases, respectively; the k^* values of 1.2 for HCHO and 1.5 for HF were significantly lower than those of the C2-DMA film. Thus, the use of an amine-based crosslinked film could lead to a highly sensitive response to, and an improved selectivity for, HCl gas.

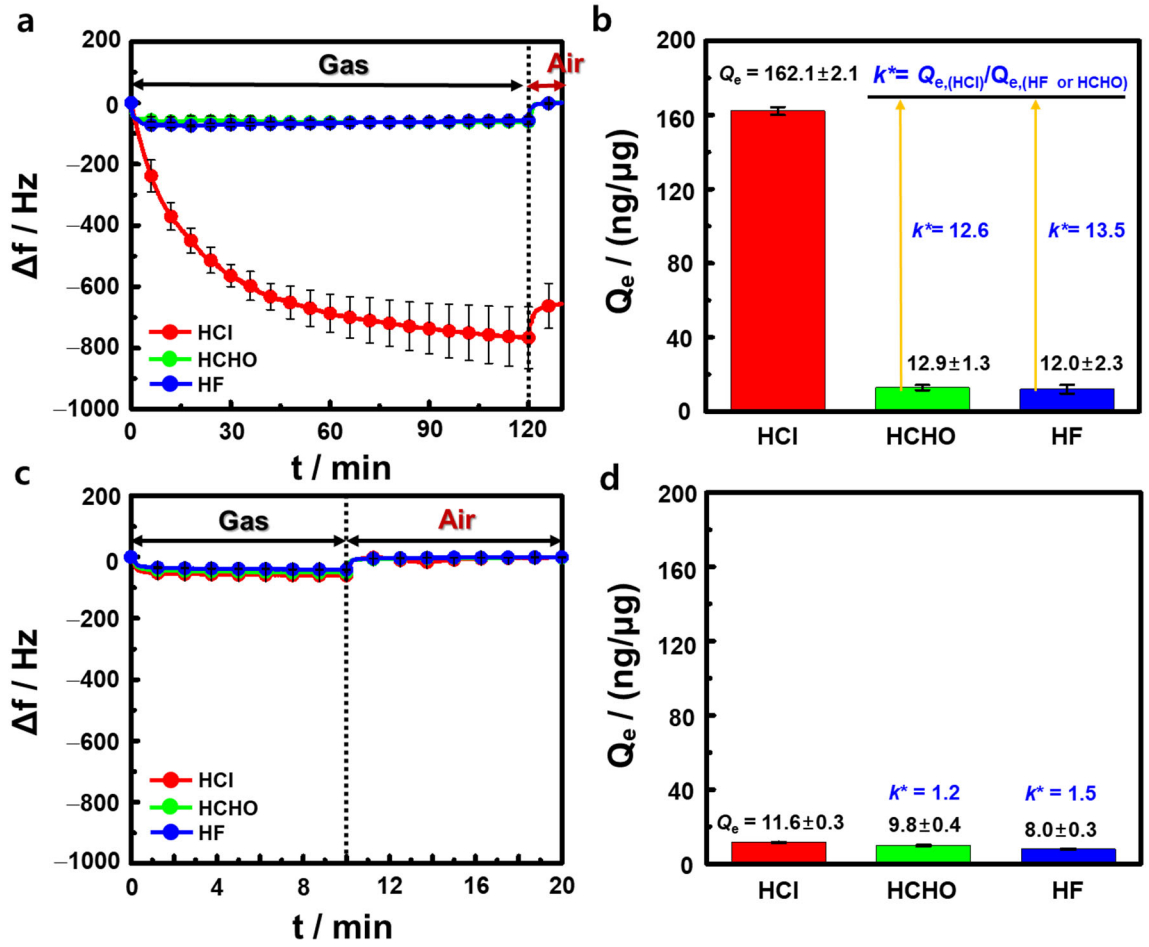

Figure 6. (**a**) Resonant frequency change (Δf) for poly(DMAEMA-co-EGDMA) film as a function of time in flow of 70-ppm different gases (HCl, HCHO, and HF), at 22 °C and 10% RH, during a 2-h adsorption process and (**b**) 2D bar plot of equilibrium binding capacity (Q_e) as a function of toxic gas types in flow of 70-ppm different gases (HCl, HCHO, and HF). (**c**,**d**) Resonant frequency change (Δf) for poly(DMAA-co-EGDMA) film as a function of time in gas flow, and equilibrium binding capacity (Q_e) as a function of toxic gas type during a 10-min adsorption process under the same gas flow conditions.

4. Conclusions

In this study, crosslinked C0-DMA and C2-DMA films were successfully manufactured on QC electrodes for the adsorption of HCl gas via photopolymerization. Their adsorption response (Q_e) was strongly dependent on film mass, and their mass was optimized in order to obtain maximum adsorption of HCl molecules. Regarding the optimized film mass, the Q_e value (161.7 ± 2.8 ng/μg) of the C2-DMA film was 13.9-fold higher than that of the C0-DMA film (Q_e = 11.6 ± 0.3 ng/μg) when 70-ppm HCl was flown through a chamber. The adsorption response of the C2-DMA film was unaffected by specific atmospheric conditions (synthetic air or N_2 gas) during the HCl adsorption process because the film had a strong interaction with HCl gas through protonation and ionic bonding.

Furthermore, the film showed an 14.8-fold higher sensitivity (2.51 [ng/μg][1/ppm]), and a higher selectivity coefficient (k^*) (12.6-fold for HCHO gas and 13.5-fold for HF gas), than the C0-DMA film. Thus, the dimethylamine-based crosslinked copolymer films could be used as highly sensitive and selective HCl gas sensors which are inexpensive and easy to produce.

Supplementary Materials: The following supporting information can be downloaded at https://www.mdpi.com/article/10.3390/chemosensors10020070/s1. Figure S1: Cross-sectional scanning electron microscopy (SEM) images of poly(DMAEMA-co-EGDMA) films with mass of (a) 1.7 μg and (b) 11.8 μg, respectively. All scale bars are 1 μm. Figure S2: Resonant frequency change (Δf) as a function of time for poly(DMAEMA-co-EGDMA) and poly(DMAA-co-EGDMA) films in 70-ppm HCl, and synthetic air flow at 22 °C (10% RH). The adsorption–desorption process was performed until the signal stabilized. Figure S3: Resonant frequency change (Δf) as a function of time for poly(DMAEMA-co-EGDMA) and poly(DMAA-co-EGDMA) films in 100-ppm HCl and N_2 flow at 22 °C (10% RH). A three cycle adsorption–desorption process was performed. Figure S4: XPS wide scan spectra for poly(DMAEMA-co-EGDMA) and poly(DMAA-co-EGDMA) films before and after HCl adsorption. Figure S5: Resonant frequency change (Δf) as a function of time for (a) poly(DMAEMA-co-EGDMA) and (b) poly(DMAA-co-EGDMA) films in HCl gas flow ranging from 10 to 70 ppm, at 22 °C and 10% RH during the adsorption process. Synthetic air was used for desorption, and the desorption process was performed until the signal stabilized. Figure S6: Linear regression curve of poly(DMAEMA-co-EGDMA) for resonant frequency change (Δf) as a function of HCl concentration in HCl ranging from 10 to 50 ppm. Table S1: Comparison of HCl on various sensor configurations, including the sensitivity and limit of detection in a linear range [14,17,19,22,32]. Table S2: Fitting parameters of the Langmuir and Freundlich models for the adsorption of HCl gas on two crosslinked films.

Author Contributions: Conceptualization, J.Y. and J.P.; methodology, J.Y. and J.P.; validation, J.P.; formal analysis, J.Y. and J.P.; investigation, J.Y.; data curation, J.Y.; writing—original draft preparation, J.P.; visualization, J.Y. and J.P.; supervision, J.P.; funding acquisition, J.P. All authors have read and agreed to the published version of the manuscript.

Funding: This work was supported by the Ministry of Trade, Industry and Energy, Republic of Korea (Grant No. N0002310).

Institutional Review Board Statement: Not applicable.

Informed Consent Statement: Not applicable.

Data Availability Statement: Not applicable.

Conflicts of Interest: The authors declare no conflict of interest.

References

1. Wang, K.-S.; Chiang, K.-Y.; Lin, S.-M.; Tsai, C.-C.; Sun, C.-J. Effects of chlorides on emissions of hydrogen chloride formation in waste incineration. *Chemosphere* **1999**, *38*, 1571–1582. [CrossRef]
2. Bal, M.; Biswas, S.; Behera, S.K.; Meikap, B.C. Modeling and optimization of process variables for HCl gas removal by response surface methodology. *J. Environ. Sci. Health A Tox. Hazard. Subst. Environ. Eng.* **2019**, *54*, 359–366. [CrossRef] [PubMed]
3. Heggie, T.W. Geotourism and volcanoes: Health hazards facing tourists at volcanic and geothermal destinations. *Travel Med. Infect. Dis.* **2009**, *7*, 257–261. [CrossRef]
4. Hu, M.; Kang, W.; Cheng, B.; Li, Z.; Zhao, Y.; Li, L. Sensitive and fast optical HCl gas sensor using a nanoporous fiber membrane consisting of poly (lactic acid) doped with tetraphenylporphyrin. *Microchim. Acta* **2016**, *183*, 1713–1720. [CrossRef]
5. Hu, M.; Kang, W.; Zhao, Y.; Shi, J.; Cheng, B. A fluorescent and colorimetric sensor based on a porphyrin doped polystyrene nanoporous fiber membrane for HCl gas detection. *RSC Adv.* **2017**, *7*, 26849–26856. [CrossRef]
6. Xie, Y.-Z.; Shan, G.-G.; Zhou, Z.-Y.; Su, Z.-M. Schiff-base as highly sensitive and reversible chemosensors for HCl gas. *Sens. Actuators B Chem.* **2013**, *177*, 41–49. [CrossRef]
7. Jeon, H.; Lee, J.; Kim, M.H.; Yoon, J. Polydiacetylene-based electrospun fibers for detection of HCl gas. *Macromol. Rapid Commun.* **2012**, *33*, 972–976. [CrossRef]
8. Muthukumar, P.; John, S.A. Highly sensitive detection of HCl gas using a thin film of meso-tetra(4-pyridyl)porphyrin coated glass slide by optochemical method. *Sens. Actuators B Chem.* **2011**, *159*, 238–244. [CrossRef]
9. Park, Y.K.; Oh, H.J.; Bae, J.H.; Lim, J.Y.; Lee, H.D.; Hong, S.I.; Son, H.S.; Kim, J.H.; Lim, S.J.; Lee, W. Colorimetric textile sensor for the simultaneous detection of NH_3 and HCl gases. *Polymers* **2020**, *12*, 2595. [CrossRef]

10. Owyeung, R.E.; Panzer, M.J.; Sonkusale, S.R. Colorimetric gas sensing washable threads for smart textiles. *Sci. Rep.* **2019**, *9*, 5607. [CrossRef] [PubMed]
11. Imaya, H.; Ishiji, T.; Takahashi, K. Detection properties of electrochemical acidic gas sensors using halide–halate electrolytic solutions. *Sens. Actuators B Chem.* **2005**, *108*, 803–807. [CrossRef]
12. Chen, J.; Yang, J.; Yan, X.; Xue, Q. NH_3 and HCl sensing characteristics of polyaniline nanofibers deposited on commercial ceramic substrates using interfacial polymerization. *Synth. Met.* **2010**, *160*, 2452–2458. [CrossRef]
13. Murugappan, K.; Silvester, D.S. Electrochemical studies of hydrogen chloride gas in several room temperature ionic liquids: Mechanism and sensing. *Phys. Chem. Chem. Phys.* **2016**, *18*, 2488–2494. [CrossRef] [PubMed]
14. Matsuguchi, M.; Kadowaki, Y. Poly(acrylamide) derivatives for QCM-based HCl gas sensor applications. *Sens. Actuators B Chem.* **2008**, *130*, 842–847. [CrossRef]
15. Lakard, B.; Carquigny, S.; Segut, O.; Patois, T.; Lakard, S. Gas sensors based on electrodeposited polymers. *Metals* **2015**, *5*, 1371–1386. [CrossRef]
16. Xu, N.; Wang, R.-L.; Li, D.-P.; Zhou, Z.-Y.; Zhang, T.; Xie, Y.-Z.; Su, Z.-M. Continuous detection of HCl and NH_3 gases with a high-performance fluorescent polymer sensor. *New J. Chem.* **2018**, *42*, 13367–13374. [CrossRef]
17. Matsuguchi, M.; Harada, N.; Omori, S. Poly(N-isopropylacrylamide) nanoparticles for QCM-based gas sensing of HCl. *Sens. Actuators B Chem.* **2014**, *190*, 446–450. [CrossRef]
18. Matsuguchi, M.; Tada, A. Fabrication of poly(N-isopropylacrylamide) nanoparticles using a simple spray-coating method and applications for a QCM-based HCl gas sensor coating. *Sens. Actuators B Chem.* **2017**, *251*, 821–827. [CrossRef]
19. Matsuguchi, M.; Fujii, S. HCl gas sensor coating based on poly (N-isopropylacrylamide) nanoparticles prepared from water-methanol binary solvent. *Sensors* **2018**, *18*, 3283. [CrossRef]
20. Matsuguchi, M.; Takaoka, K.; Kai, H. HCl gas adsorption/desorption properties of poly (N-isopropylacrylamide) brushes grafted onto quartz resonator for gas-sensing applications. *Sens. Actuators B Chem.* **2015**, *208*, 106–111. [CrossRef]
21. Zhao, X.J.; Gao, Z.F.; Jiang, Z.Y. A study of HCl gas adsorption/desorption properties of PNIPAM brushes. *Macromol. Theory Simul.* **2015**, *24*, 460–467. [CrossRef]
22. Jin, Y.-J.; Park, J. QCM-based HCl gas sensors using spin-coated aminated polystyrene colloids. *Polymers* **2020**, *12*, 1591. [CrossRef] [PubMed]
23. Sauerbrey, G.Z. The use of quartz oscillators for weighing thin layers and for microweighing. *Z. Phys.* **1959**, *155*, 206–222. [CrossRef]
24. Jie, Z.; Yan, X.; Zhao, L.; Worley, S.D.; Liang, J. Eco-friendly synthesis of regenerable antimicrobial polymeric resin with N-halamine and quaternary ammonium salt groups. *RSC Adv.* **2014**, *4*, 6048–6054. [CrossRef]
25. Kim, D.; Subramanian, S.; Thirion, D.; Song, Y.; Jamal, A.; Otaibi, M.S.; Yavuz, C.T. Quaternary ammonium salt grafted nanoporous covalent organic polymer for atmospheric CO_2 fixation and cyclic carbonate formation. *Catal. Today* **2020**, *356*, 527–534. [CrossRef]
26. Hajir, M.; Dolcet, P.; Fischer, V.; Holzinger, J.; Landfester, K.; Muñoz-Espí, R. Sol–gel processes at the droplet interface: Hydrous zirconia and hafnia nanocapsules by interfacial inorganic polycondensation. *J. Mater. Chem.* **2012**, *22*, 5622–5628. [CrossRef]
27. Pascal-Delannoy, F.; Sorli, B.; Boyer, A. Quartz crystal microbalance (QCM) used as humidity sensor. *Sens. Actuators B Chem.* **2000**, *84*, 285–291. [CrossRef]
28. Gupta, V.K.; Yola, M.L.; Atar, N. A novel molecular imprinted nanosensor based quartz crystal microbalance for determination of kaempferol. *Sens. Actuators B Chem.* **2014**, *194*, 79–85. [CrossRef]
29. Diñeiro, Y.; Menéndez, M.I.; Blanco-López, M.C.; Lobo-Castañón, M.J.; Miranda-Ordieres, A.J.; Tuñón-Blanco, P. Computational predictions and experimental affinity distributions for a homovanillic acid molecularly imprinted polymer. *Biosens. Bioelectron.* **2006**, *22*, 364–371. [CrossRef]
30. Li, Z.; Li, J.; Guo, Z.; Campos, L.C. Investigation of metaldehyde removal by powdered activated carbon from different water samples. *Environ. Sci. Water Res. Technol.* **2020**, *6*, 1432–1444. [CrossRef]
31. Li, X.; Liu, H.; Deng, Z.; Chen, W.; Li, T.; Zhang, Y.; Zhang, Z.; He, Y.; Tan, Z.; Zhong, S. PEGylated thermo-sensitive bionic magnetic core-shell structure molecularly imprinted polymers based on halloysite nanotubes for specific adsorption and separation of bovine serum albumin. *Polymers* **2020**, *12*, 536. [CrossRef] [PubMed]
32. Matsuguchi, M.; Kadowaki, Y.; Noda, K.; Naganawaet, R. HCl gas monitoring based on a QCM using morpholine-functional styrene-co-chloromethylstyrene copolymer coatings. *Sens. Actuators B Chem.* **2007**, *120*, 462–466. [CrossRef]